

# Dynamics of Grain Boundaries in Two-Dimensional Hydrogen-Bonded Molecular Networks\*\*

Markus Lackinger,\* Stefan Griessl, Lorenz Kampschulte, Ferdinand Jamitzky, and Wolfgang M. Heckl

*The temporal evolution of domain boundaries of hydrogen-bonded molecular monolayers at the liquid–solid interface is evaluated by recording series of subsequent scanning tunneling microscopy (STM) images. Comparison of dissimilar benzene carboxylic acids reveals a clear distinction between one- and two-dimensional H-bonded network structures. Trimesic acid forms a two-dimensionally H-bonded networked structure, whereas terephthalic acid organizes in a dense packing of H-bonded linear chains on a graphite surface. In addition, TMA forms a sixfold lattice on a threefold graphite substrate, whereas TPA exhibits only a twofold lattice, causing a high grain-boundary line energy for the latter. In the case of TMA the nanostructure was mostly stable during the observation time. For TPA, Ostwald ripening—that is, the growth of larger islands at the expense of smaller islands—was observed. To explain the various experimentally observed timescales of the dynamics occurring at grain boundaries, molecular mechanics simulations were applied to calculate the binding energy of edge molecules, that is, the line energy, of finite islands of both trimesic and terephthalic acid on a graphite substrate.*

## Keywords:

- hydrogen bonding
- molecular dynamics
- molecular mechanics
- self-assembly
- structure–property relationships


## 1. Introduction

Many technologically relevant materials are applied in a polycrystalline state, that is, the active region of the material

consists of grains with a more- or less-defined size, shape, and orientation. Nucleation (the density and spatial distribution of the nuclei) as the first step of crystal growth determines the average size and distribution of the crystallites.<sup>[1]</sup> Given sufficient thermal energy, a reorganization of the nanostructure can still take place. For two-dimensional (2D) molecular layers on atomically clean substrates, homonucleation (nuclei comprised of at least a critical number of crystallizing species) generally occurs, and monolayer growth is terminated when grains touch one another. This process generates grain boundaries that limit the translational symmetry of the otherwise crystalline material. Hence, this kind of defect has a high impact on important physical properties, in particular transport properties such as electrical conductivity. STM has already proven its value for the investigation of inorganic grain boundaries,<sup>[2]</sup> and similarly for studies on the structure and dynamics of grain boundaries in organic monolayers.<sup>[3]</sup>

[\*] Dr. M. Lackinger, Dr. S. Griessl, L. Kampschulte, Dr. F. Jamitzky, Prof. W. M. Heckl  
Ludwig-Maximilians-Universität München  
Departement für Geo- und Umweltwissenschaften & Center for NanoScience (CeNS)  
Theresienstr. 41, 80333 München (Germany)  
Fax: +49 89 2180 4331  
E-mail: markus@lackinger.org  
Prof. W. M. Heckl  
Deutsches Museum  
80306 München (Germany)

[\*\*] We thank the DFG for financial support within the SFB 486 “manipulation of matter on the nanoscale” and Paul Hix for proofreading.

 Supporting information for this article is available on the WWW under <http://www.small-journal.com> or from the author.

Depending on the ratio between available thermal energy and binding energy of the building blocks of the crystal adjacent to the grain boundary, dynamics and reorganization can occur; particles can fluctuate between neighboring grains without generating a net flux. Alternatively, larger grains can grow at the expense of smaller ones—a process known as Ostwald ripening. Moreover, adjacent grains can coalesce and form a more extended island through the incorporation of additional material.

The subjects of this study are 2D hydrogen-bonded supramolecular structures at the liquid–solid interface. Here, organic molecules adsorb and self-assemble on a solid substrate with the liquid phase above. The liquid phase serves as a reservoir for molecules and is normally in a dynamic equilibrium with the molecular layer on the surface. Herein we focus on hydrogen-bonded molecular systems. Because of their relative strength in comparison to pure Van der Waals bonds, H-bonds are very important both in nature and in the design of supramolecular structures.<sup>[4]</sup> Another interesting aspect, which can be exploited for tailoring supramolecular structures, is the selectivity and directionality of H-bonds.<sup>[5]</sup> Herein, we compare networks of 1,3,5-benzene-tricarboxylic acid (trimesic acid; TMA) and 1,4-benzene-dicarboxylic acid (terephthalic acid; TPA) at the interface between the respective solution and the (0001) plane of highly oriented pyrolytic graphite with heptanoic acid as solvent. TPA forms densely packed molecular chains,<sup>[6]</sup> whereas TMA builds a 2D H-bonded network.<sup>[7]</sup> Models of both structures are depicted in Figure 1. In this work, in situ STM was used as a high-resolution real-space observation tool. By means of video-STM (that is, merging subsequent STM “snapshots” into a movie, similar to making a flipbook), changes in island size and shape on a timescale of ten minutes are visualized (for details see the Experimental Section). Likewise, Rabe and co-workers investigated Ostwald ripening in 2D molecular layers at the liquid–solid interface.<sup>[8]</sup> In one work two different systems exhibit Ostwald

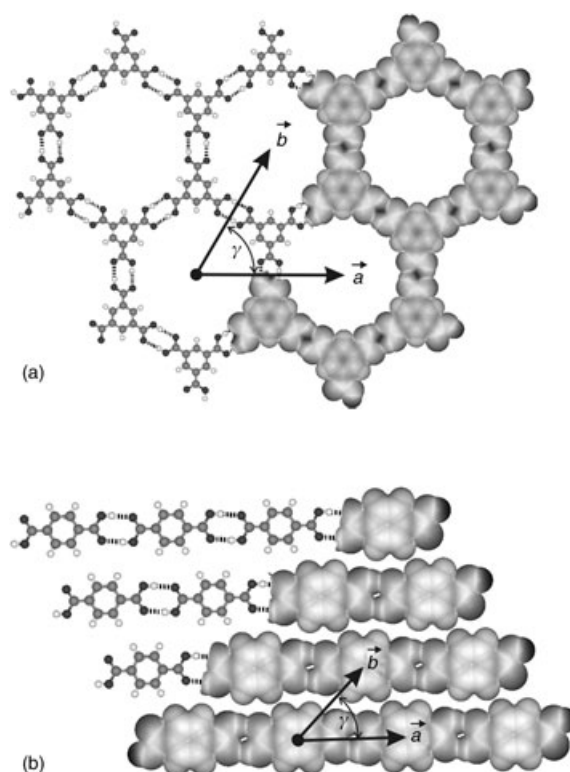


**Figure 1.** Models of the monolayer structures of a) trimesic acid (TMA) and b) terephthalic acid (TPA) on graphite; on the right-hand side the molecules are depicted with the Van der Waals radii of the atoms; the black dashed lines indicate hydrogen-bonds, where two H-bonds are formed between adjacent carboxylic groups; each TPA molecule within the monolayer is bound by a total of four H-bonds, whereas each TMA molecule forms six H-bonds. The lattice parameters for TMA and TPA are  $a = b = 1.6$  nm,  $\gamma = 60^\circ$  and  $a = 1.0$  nm,  $b = 0.9$  nm and  $\gamma = 46^\circ$ , respectively.

ripening on slightly different timescales, whereas here TPA rearranges very rapidly and the TMA nanostructure remains almost unaffected, at least during the observation time.



**Editorial Advisory Board Member**

Wolfgang M. Heckl is the general director of the Deutsches Museum in Munich, and Professor at the Ludwig Maximilians University (LMU), where he is head of an interdisciplinary research group in nanobiosciences. He received his PhD (1988) in biophysics from the Technical University of Munich and did postdoctoral studies at the Max Planck Institute for quantum optics in Garching and at the University of Toronto. He also participated in an IBM research group, where he

worked with Nobel Laureate Gerd Binnig. He received the Philip Morris research award (1993) for the first real-space images of DNA bases, the Communicator Award of the German Science Foundation (2002), and the Descartes Prize for Science Communication of the European Commission (2004). He is a member of the Center for NanoScience (CeNS) and the GeoBioCenter at Munich University, as well as a founding member and the spokesman of the Excellence Network NanoBioTechnology.

**2. Results and Discussion**

In thermodynamic equilibrium both TMA and TPA molecules assemble in long-range-ordered monolayers at the interface between the heptanoic acid solution and the (0001) face of a highly oriented pyrolytic graphite substrate. The unit cells of the systems under investigation are already known from previous studies. TMA forms a sixfold-symmetric hydrogen-bonded network, with each TMA molecule bound to three neighboring molecules,<sup>[7]</sup> whereas TPA assembles in linear, 1D H-bonded chains, which are associated mainly through comparatively weak Van der Waals forces.<sup>[6]</sup> Since carboxylic groups can act as both a donor and acceptor for H-bonds, intermolecular bonding becomes possible without the need for further functional groups. Two H-bonds are formed per two adjacent carboxylic groups, and a straight configuration, that is, a bonding angle of  $180^\circ$ , is energetically most favorable. In contrast to TPA, TMA assembles in an open (that is, not densely packed) structure with

a periodic arrangement of voids, suitable for the incorporation of both TMA and different species as guest molecules. As shown previously, these voids are appropriate for the co-adsorption of coronene and buckminsterfullerenes.<sup>[9]</sup>

The dynamics at grain boundaries were analyzed by means of a series of subsequent STM images. In this paper only a few snapshots are shown, but whole series, packed into movies, are available as Supporting Information.<sup>[10]</sup>

For TMA, a series of 47 subsequent STM images was recorded; selected snapshots are presented in Figure 2a–c). The recording time for a single frame was approximately 20 s. Hence the whole movie (TMA1.mov, see Supporting Information) covers a time span of approximately 16 min. This series reveals fluctuations at domain boundaries between rotational and anti-phase domains. Rotational domains are characterized by different azimuthal orientations of the adsorbate lattice vectors (for example, the two domains at the left-hand side of Figure 2), whereas anti-phase domains are laterally translated by an integer number of substrate lattice vectors, although their extrapolated lattices do not coincide; an example is given by the two domains on

the right-hand side of Figure 2. It was found in previous studies that the primitive TMA lattice vectors, as sketched in Figure 1a, are tilted  $\pm 5^\circ$  with respect to the graphite  $[\bar{1}2\bar{1}0]$  directions, which gives rise to two energetically equivalent rotational domains. The resulting incommensurability leads to a Moiré-like sixfold superstructure with a lattice constant of  $\approx 10$  nm, which can be recognized as a modulation of the apparent height in the STM images of Figure 2. The superstructure unit cell is marked by arrows in Figure 2b. To allow the superstructure to be discerned more easily, a different color coding was applied to the domain at the lower right side. Substrate-induced Moiré patterns are well known from other adsorbate–substrate combinations.<sup>[11]</sup> Since the graphite substrate exhibits a threefold symmetry and the adsorbate a sixfold symmetry only two different, equally favored rotational domains exist.

In the STM images of TMA grain boundaries, only fluctuations without a lasting exchange of molecules were observed. Single six-membered TMA rings build up and decay again at the domain boundaries; it essentially appears that the molecules are just going back and forth between adja-

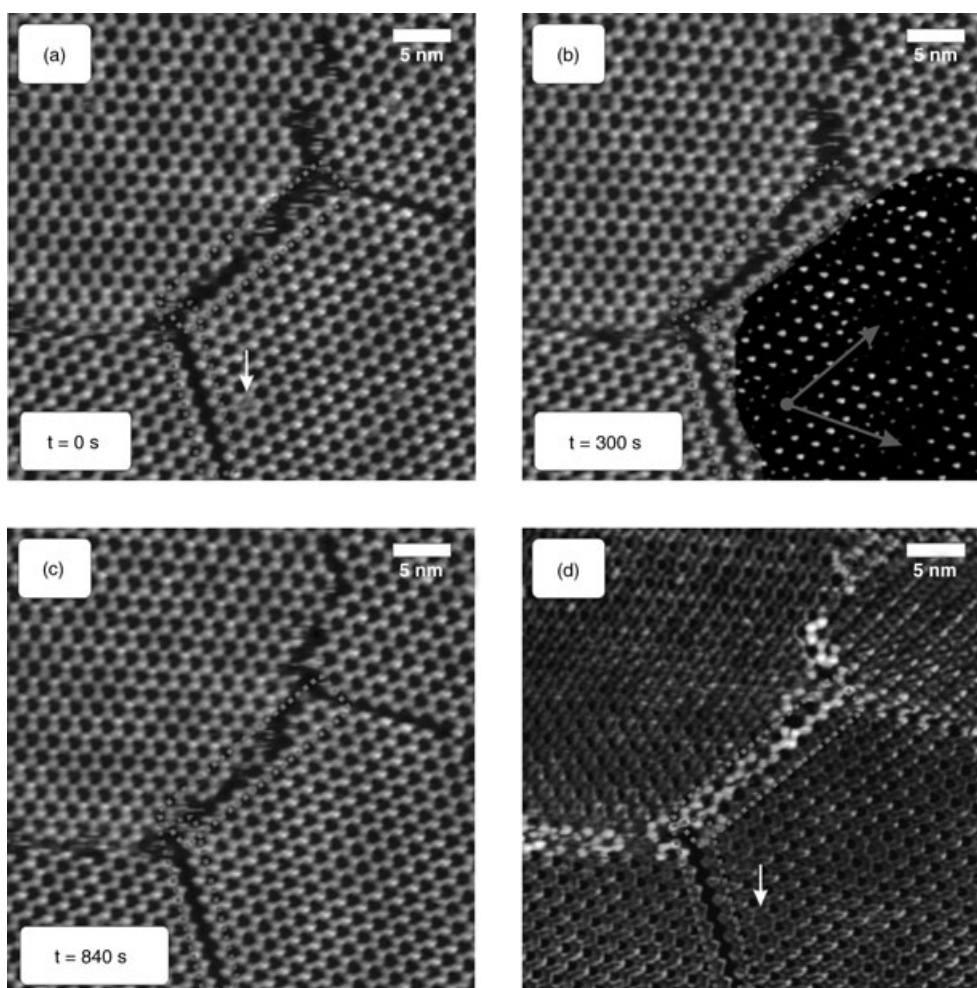


**Figure 2.** a–c) Selected snapshots of a series of STM images of TMA domain boundaries ( $40 \times 40 \text{ nm}^2$ ). Only slight changes happen directly at the domain edge and the domain size and shape is mainly preserved; d) standard deviation of all 47 images of the series. Brighter shading indicate larger values of the standard deviation, and therefore represents regions that exhibit enhanced molecular dynamics. The Moiré pattern in (b) is discerned by the color coding of the island at the lower right. Arrows indicate the vectors of the sixfold superstructure. See the Supporting Information for color images.<sup>[10]</sup>

cent domains. Single molecules cannot be tracked here, although in particular cases, this becomes possible through chemically marked molecules.<sup>[12]</sup> Thus, a mechanism with desorption at one domain boundary and adsorption at the other cannot be excluded. However, the observation that the uncovered area between the domains remains nearly constant throughout the observation time favors the hypothesis of an exchange between the domains, rather than correlated adsorption/desorption events. An example is marked in Figure 2a–c) by the dashed rectangle in the center of the image. For this reason the shape and size of the TMA islands (that is, the nanostructure) is mainly preserved throughout the observation time. The close-packed domain boundaries between the two translated domains (marked by the second dashed rectangle) in the lower part of the image do not show any fluctuations at all and are extraordinarily stable. Apparently, dense-packed edges of TMA domains without any kinks are stable at room temperature.

In order to illustrate the fluctuations occurring in all frames in a single image, the standard deviation of 47 aligned images is shown in Figure 2d. The color coding of each pixel represents the value of the standard deviation of this pixel from all STM images at this position. During image acquisition it was necessary to compensate for drift; details are given in the Experimental Section. In principle, this standard deviation image represents a mapping of the dynamics. It can be seen that those non-close-packed domain boundaries exhibit a high value of the standard deviation (bright in the image and marked by the dashed rectangle in the center) and therefore indicate molecular fluctuations. In contrast, the close-packed anti-phase domain boundary in the lower right part (marked by the second dashed rectangle) of the image does not show any fluctuations at all in the standard deviation image. This more condensed view of the dynamics in the standard deviation image is also consistent with the STM movie (TMA1.mov), where single six-membered TMA rings assemble and disassemble at the domain edge during the time of observation. As evident in Figure 2d the standard deviation mimics the TMA lattice as well. The reason for this is a residual misalignment, which can be attributed to an imperfect drift correction during the measurement. Due to changes in the drift and/or superimposed drift correction, the measured lattice parameters, both length and angles, are slightly distorted and cannot be compensated for just by lateral alignment.

In the STM movie (TMA1.mov) some TMA cavities within the network show a transient adsorption of a molecular guest from the liquid phase. An example is marked in Figure 2a by the white arrow. An occupation of a TMA cavity during a single scanning frame is sufficient to be recognized in the standard deviation, with the white arrow in Figure 2d pointing to the very same cavity. These guests are most likely TMA molecules, likewise observed within the cavities of evaporated TMA films.<sup>[7]</sup> They can interact with the TMA lattice by means of weak H-bonds. However, since they are observed so rarely, their stabilization energy must be considerably lower. A detailed analysis of TMA as a guest molecule in the TMA chicken-wire polymorph will be published elsewhere.

It is also obvious that fluctuations of the TMA structure are spatially limited to the region of the domain boundary up to the first dense-packed edge of the TMA domain, which results in conservation of the island shape and size. In a second STM movie of TMA (TMA2.mov) however, one island grows at the expense of a rather small one (diameter  $\approx 20$  nm, marked by the dashed black circle in the first frame of the movie). This might be explained by the high ratio of edge molecules in these small islands. In other words, the relatively high line-energy of small islands, that is, the high ratio of circumference to area, renders them thermodynamically unstable. This process can be understood in the framework of Ostwald ripening. However, in the case of TMA, it was only observed for rather small islands. A further event in this movie is the coalescence of two islands (the respective grain boundary is marked by black arrows in the first frame of the movie). This can only happen if these are true domains (with the same rotational orientation and no translational displacement, that is, their extrapolated lattices coincide) by adsorption of linking TMA molecules from the liquid phase, thereby filling the gap between these two domains. Otherwise the merger of these two islands would have to be accompanied by a 1D defect, such as a dislocation.

In comparison, the TPA nanostructure is not quite as stable as that of TMA at the same temperature on a comparable timescale. Experimental evidence is given in Figure 3a–d) and the movie TPA1.mov by a sequence of STM images, where a smaller island with different rotational orientation is incorporated into the surrounding domain. This event can be seen as an example for the more general concept of Ostwald ripening. Again, the driving force is the minimization of free energy by avoiding additional energy costs at grain boundaries due to line energy. The smaller island, because of its higher circumference-to-area ratio, is thermodynamically less stable. The small hole in the monolayer shown in Figure 3d, which was left after the island had disappeared, was observed for an additional  $\approx 10$  min (TPA2.mov) until it was entirely closed by adsorption from the liquid phase. Although there is a huge number of TPA molecules offered in the liquid phase above, it takes a considerable amount of time to adsorb enough TPA molecules to finally close the hole. The movie TPA2.mov shows that many adsorption and desorption processes are actually necessary until a stable configuration is reached. On average, approximately 14 TPA adsorption sites are unoccupied during the movie with a standard deviation of  $\approx 4$  adsorption sites. The number of free adsorption sites in the hole versus time is depicted in Figure 4. Because the number of unoccupied TPA adsorption sites varies non-monotonically, it is assured that adsorption and desorption actually happens, but rearrangement of the TPA molecules within the hole might play a role as well. The lifetime of this hole is remarkably long. One possible explanation is offered by the kinetics of the system. A low concentration and/or mobility of TPA in the liquid phase would explain an exceedingly long life time. However, since TPA desorption events are observed as well (compare Figure 4), it is more likely that the hole can be considered as a separate 2D molecular gas

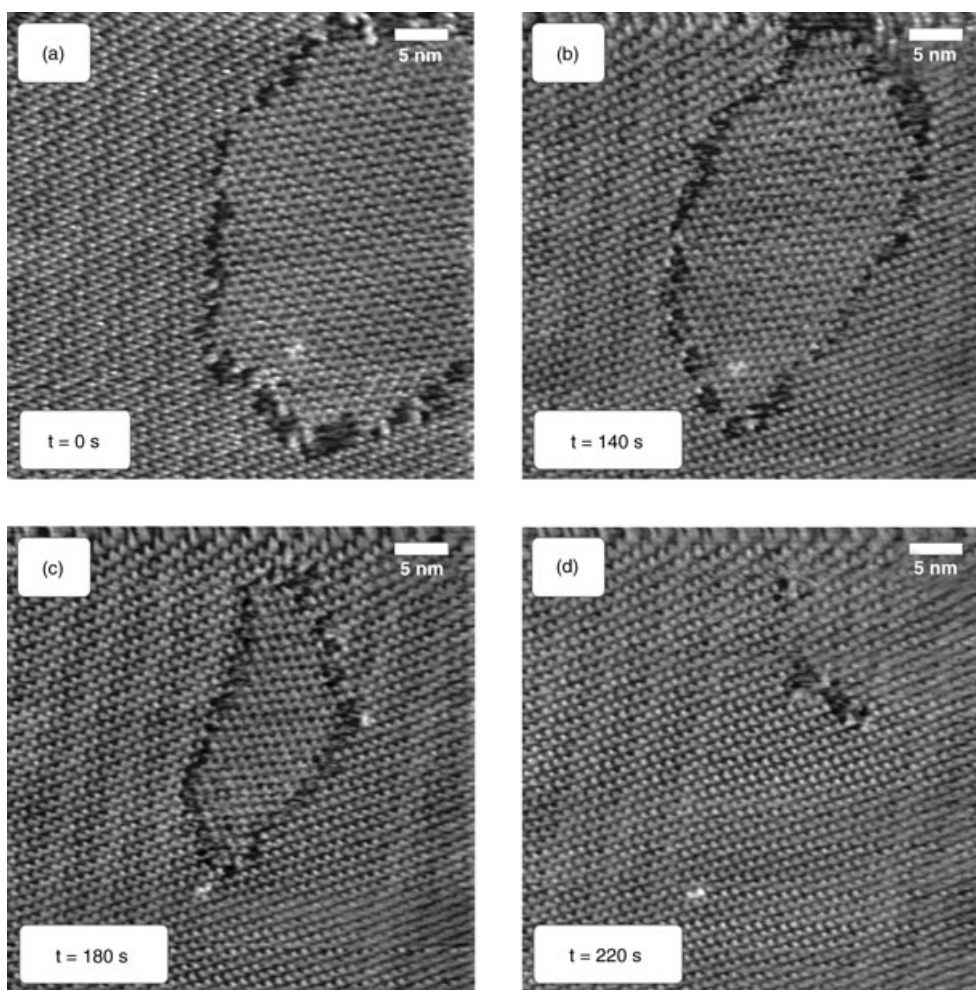


**Figure 3.** Series of STM topographs ( $43 \times 43 \text{ nm}^2$ ) of a TPA monolayer on graphite (0001). The images show a small island surrounded by a domain with different rotational orientation. From (a) to (c) the surrounding area is growing at expense of the small island until only a small hole with a size on the order of 10 TPA adsorption sites is left (d).

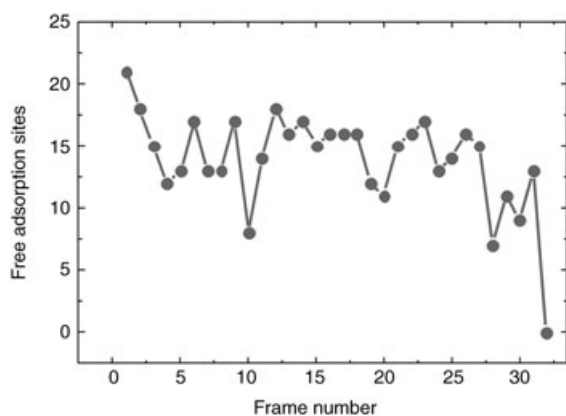


**Figure 4.** Number of free adsorption sites (corresponding to the size of the hole in Figure 3 d) versus frame number (one frame represents  $\approx 20 \text{ s}$ ). The graph shows that adsorption (negative slope) and desorption (positive slope) events actually take place. Thus the number of free adsorption sites does not demonstrate a monotonic time dependence. The mean number of free adsorption sites amounts to  $\approx 14$  and the standard deviation to  $\approx 4$ .

phase in equilibrium with the 2D crystalline phase. Because this separate phase has an average size of only 14 adsorption sites, it is too small to be thermodynamically stable and eventually disappears. STM images of the TPA monolayer on a larger scale and at different locations show both very large domains and small holes comparable to that shown in Figure 3 d, which suggests the mechanism under discussion is important for reorganization processes in the TPA monolayer. Comparable small holes were found in domains of the equally 1D H-bonded networks of 2,6-naphthalene-dicarboxylic acid (NDA). Since the adsorption energy of NDA on graphite is larger due to its more extended  $\pi$ -electron system, the reorganization of the molecules takes place on a longer timescale. However, the appearance of comparable small holes within NDA islands might be a hint for a more general grain-coarsening mechanism in 1D H-bonded adsorbate layers.

The driving force for the disappearance of the smaller enclosed TPA island is of thermodynamic origin, namely the minimization of the free energy by the elimination of domain boundaries, which cause additional energy costs due to their line energy. But what is the physical reason that

domain boundaries of the TMA network are stable for several 10 min, whereas TPA domain boundaries reorganize and even vanish within several minutes? Apparently this experimental observation must be related to the line energies of both structures. From the models in Figure 1 it is evident that the sixfold symmetry of the TMA lattice results in three equivalent dense-packed domain boundaries with angles of  $120^\circ$  and  $240^\circ$  between each other, respectively. On the contrary, the TPA structure only has a twofold symmetry. This fact leads to two vastly different domain boundaries, where edge molecules differ in the number of formed H-bonds and consequently their binding energy. Thus, TPA domains exhibit facets with a considerably lower binding energy of the edge molecules, which gives rise to the observed highly dynamic behavior.

In order to obtain a quantitative estimate for the binding energies of edge molecules, molecular mechanics simulations with a Dreiding II force field,<sup>[13]</sup> which includes a specific term for H-bonding, were performed. First, the orientations of the molecules within the unit cells were determined by applying periodic boundary conditions and using the lattice parameters determined by calibrated STM measurements as a constraint.<sup>[6]</sup> The calibration was achieved by recording images with one half showing the adsorbate layer and the other half the substrate lattice, thereby using the atomic lattice of the substrate as an intrinsic ruler. The fast Fourier transform (FFT) of these split images allows for a precise determination of the superstructure matrix. The following energy minimization yields refined information about the orientation of the molecules within the unit cell. According to Figure 1 the TMA structure has two molecules per primitive unit cell, while TPA only has one. These optimized unit cells were used as a base to create finite islands as depicted in Figure 5. In order to include edge effects like structural relaxation due to the lower coordination of edge molecules, an additional energy minimization of the finite islands was performed. For this second minimization molecules within the island, which are sufficiently far away from the edge, were kept fixed. Finally, the binding energy of the various edge and corner molecules was calculated as the difference in total energies for configurations with the molecule under consideration in place and when “infinitely” far away. In this case the “binding energy” is comprised of the sum of lateral binding and desorption energies. In these calculations the influence of the liquid phase above is neglected. However, a comparison of TPA and TMA edge-binding energies is justified. The corresponding binding energies are depicted in Figure 5 for both TMA and TPA. The intuitively attributed higher stability of the TMA domain boundary is confirmed by the molecular mechanics simulations. One type of edge molecule exhibit a total of four H-bonds (two per carboxylic group) and a relatively high binding energy of 1.87 eV, while the second type of edge molecule is sixfold H-bonded, and the binding energy amounts to 2.21 eV due to the contribution of an additional two H-bonds. The situation is rather different for TPA on graphite, as shown in Figure 5b. Because of the molecular structure of TPA, a maximum of four H-bonds can be formed both within an island and at the edge, which results in a maximum binding energy

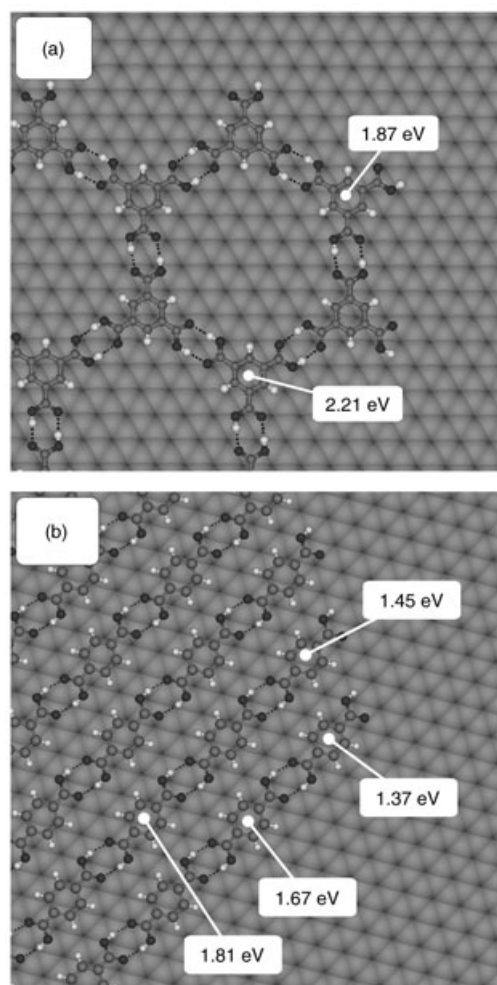


**Figure 5.** Molecular mechanics simulations of finite islands of a) TMA and b) TPA were utilized to obtain an estimate for the binding energy of edge molecules. Two adjacent carboxylic acid groups form two H-bonds, symbolized by black dotted lines. The corresponding binding energies of nonequivalent edge molecules are indicated within the models. TPA islands show two substantially differing facets with the edge molecules being bound by either two or four H-bonds, which results in a significant difference in binding energy of  $1.67 - 1.45 \text{ eV} = 0.22 \text{ eV}$ .

of 1.87 eV and 1.67 eV, respectively. However, for a finite TPA domain only two facing edges can benefit from the stabilization through four H-bonds. On the other edges TPA molecules form only two H-bonds and their binding energy is considerably lower at 1.45 eV. The TPA corner molecule is the lowest-coordinated molecule of this island and lacks Van der Waals stabilization from a second next-nearest neighbor, which is expressed in the lowest observed binding energy of 1.37 eV. These huge differences in binding energies explain the experimentally observed differences in the timescale of domain-boundary dynamics.

Although the accuracy of the absolute values of binding energies determined by purely classical molecular mechanics simulations is highly questionable—for example, the liquid phase is neglected and important interactions like mirror charges in the semimetal graphite are not included—

they are suited for a direct comparison and confirm the intuitively obvious difference in binding energies of TMA and TPA edge molecules. Most of the binding energy differences of edge molecules can be attributed to a different number of H-bonds, owing to the molecular structures and symmetries of TMA and TPA respectively. Both the experimental results and the simulations unambiguously prove the dominating influence of H-bonds in supramolecular assemblies of these rather small molecules.

### 3. Conclusions

Room-temperature video-STM at the liquid–solid interface was utilized to compare the temporal evolution of the nanostructure (that is, the molecular dynamics at grain boundaries) of one-dimensionally (TPA) versus two-dimensionally (TMA) H-bonded supramolecular structures. The 1D-networked TPA structure is comprised of densely packed, H-bonded linear chains of molecules. By means of a series of STM images it was possible to show that larger TPA domains grow at the expense of smaller domains on a timescale of minutes. The coarsening of the nanostructure can be considered as an example of the more general concept of Ostwald ripening. Since the TPA lattice exhibits only a twofold symmetry, two vastly different facets exist, with the edge molecules exhibiting a remarkable variation in binding energies. Therefore, the domain boundaries, where edge molecules are bound by two H-bonds only, are the starting points for structural changes and reorganization respectively in the monolayer. Furthermore, adsorption and desorption events within a small hole in the TPA monolayer were tracked on a single-molecule level, until the hole eventually had been entirely closed by adsorption of TPA from the liquid phase.

In comparison, due to the sixfold symmetry of the structure, TMA islands have three equivalent domain boundaries where edge molecules have even larger binding energies than in the TPA structure. The main reason is that TMA edge molecules are bound by at least four H-bonds, whereas one facet of the TPA edge molecules exhibits only two H-bonds. Consequently the TMA domain boundaries are relatively stable at room temperature, and the shape and size of islands is mainly preserved, except for very small islands. This is also in accordance with the binding energy of edge molecules as estimated for both systems by molecular mechanics simulations. In summary, by the combination of experimental results from STM measurements with theoretical calculations of edge-molecule binding energies it was possible to consistently demonstrate the relationship between symmetry, the bonding scheme of the H-bonded supramolecular structure, and the molecular dynamics at grain boundaries.

### 4. Experimental Section

All experiments were conducted at room temperature with a home-built, pocket-sized STM under ambient conditions. The microscope was driven by a commercial SPM-100 control electronics unit from RHK. Mechanically cut Pt/Ir tips were used, which were conditioned in situ by short (20–150 ms) voltage pulses. All images were obtained in the constant-current mode of operation with tunneling voltages in the range 0.5–1.5 V and reference currents of around 100 pA. Since our STM is by no means optimized for high scanning speeds, large images were recorded with a speed of  $\approx 20$  s per frame and smaller images with  $\approx 10$  s per frame. The supramolecular structures were prepared by applying a droplet of saturated solution on a freshly cleaved graphite (0001) surface. Heptanoic acid was used as a solvent for both TMA and TPA. At typical tunneling voltages this fatty acid is an insulator, and its vapor pressure is low enough for stable STM experiments in the order of 1 h. For noise reduction all images were leveled and processed with a  $3 \times 3$  Gaussian filter. In order to image the same sample area despite large drifts (mostly thermal drift) a drift-correction algorithm was essential during the measurement. For this purpose a feature of the control software, which stabilizes the position of a randomly chosen, unambiguously recognizable feature in subsequent scanning frames was used. Except for the TPA main movie (TPA1.mov), all images were additionally aligned during image processing before merging them into a movie. The maximum of the cross-correlation with a master image gives coordinates for the necessary lateral displacement. The duration of the observation period was mainly limited by the stability of the STM tip or by solvent evaporation.

In case of thermally activated processes the temperature is the most important adjustable parameter to match the timescale of the dynamics and the scanning speed. In contrast to UHV experiments the sample temperature cannot be varied greatly for experiments at the liquid–solid interface. However, for both systems under investigation the timescale of the dynamics at room temperature was appropriate to monitor changes with a scanning speed of 10–20 s per frame.

- [1] a) C. V. Thompson, *Annu. Rev. Mater. Sci.* **1990**, *20*, 245–268; b) J. E. Taylor, J. W. Cahn, C. A. Handwerker, *Acta Metall. Mater.* **1992**, *40*, 1443–1474; c) F.-J. Meyer zu Heringdorf, M. C. Reuter, R. M. Tromp, *Nature* **2001**, *412*, 517–520.
- [2] a) A. K. Kar, A. Dhar, S. K. Ray, B. K. Mathur, D. Bhattacharya, K. L. Chopra, *J. Phys. Condens. Matter* **1998**, *10*, 10795–10804; b) M. J. Rost, D. A. Quist, J. W. M. Frenken, *Phys. Rev. Lett.* **2003**, *91*, 026101–026104.
- [3] a) J. P. Rabe, S. Buchholz, *Phys. Rev. Lett.* **1991**, *66*, 2096–2099; b) R. Heinz, J. P. Rabe, W. V. Meister, S. Hoffmann, *Thin Solid Films* **1995**, *264*, 246–249; c) M. Hibino, A. Sumi, I. Hatta, *Thin Solid Films* **1996**, *273*, 272–278; d) D. Wouters, S. Hoeppeener, R. Lunckwitz, L. F. Chi, H. Fuchs, U. S. Schubert, *Adv. Funct. Mater.* **2003**, *13*, 277–280.
- [4] a) W. M. Heckl, D. P. E. Smith, G. Binnig, H. Klagges, T. W. Hansch, J. Maddocks, *Proc. Natl. Acad. Sci. USA* **1991**, *88*, 8003–8005; b) J. V. Barth, J. Weckesser, C. Cai, P. Günter, L.

- Bürgi, O. Jeandupeux, K. Kern, *Angew. Chem.* **2000**, *112*, 1285–1288; *Angew. Chem. Int. Ed.* **2000**, *39*, 1230–1234; c) M. Bohringer, K. Morgenstern, W. D. Schneider, R. Berndt, F. Mauri, A. De Vita, R. Car, *Phys. Rev. Lett.* **1999**, *83*, 324–327; d) T. Yokoyama, S. Yokoyama, T. Kamikado, *Nature* **2001**, *413*, 619–621; e) S. De Feyter, F. C. De Schryver, *Chem. Soc. Rev.* **2003**, *32*, 139–150.
- [5] a) A. Dmitriev, N. Lin, J. Weckesser, J. V. Barth, K. Kern, *J. Phys. Chem. B* **2002**, *106*, 6907–6912; b) J. Lu, Q.-d. Zeng, C. Wang, Q.-y. Zheng, L. Wana, C. Bai, *J. Mater. Chem.* **2002**, *12*, 2856–2858.
- [6] M. Lackinger, S. Griessl, T. Markert, F. Jamitzky, W. M. Heckl, *J. Phys. Chem. B* **2004**, *108*, 13652–13655.
- [7] S. Griessl, M. Lackinger, M. Edelwirth, M. Hietschold, W. M. Heckl, *Single Mol.* **2002**, *3*, 25–31.
- [8] a) A. Stabel, R. Heinz, F. C. De Schryver, J. P. Rabe, *J. Phys. Chem.* **1995**, *99*, 505–507; b) P. Samori, K. Müllen, J. P. Rabe, *Adv. Mater.* **2004**, *16*, 1761–1765.
- [9] a) S. J. H. Griessl, M. Lackinger, F. Jamitzky, T. Markert, M. Hietschold, W. M. Heckl, *J. Phys. Chem. B* **2004**, *108*, 13652–13655; b) S. Griessl, M. Lackinger, F. Jamitzky, T. Markert, M. Hietschold, W. M. Heckl, *Langmuir* **2004**, *20*, 9403–9407.
- [10] The movies (and further graphical information) are available as \*.mov files for download as Supporting Information from the *Small* website: <http://www.small-journal.com>.
- [11] a) J. P. Rabe, S. Buchholz, *Science* **1991**, *253*, 424–427; b) M. M. Reiter, F. Jamitzky, F. Trixler, W. M. Heckl, *Phys. Status Solidi A* **2001**, *187*, 171–176; c) F. Sellam, T. Schmitz-Hubsch, M. Toerker, S. Mannsfeld, H. Proehl, T. Fritz, K. Leo, C. Simpson, K. Müllen, *Surf. Sci.* **2001**, *478*, 113–121.
- [12] A. Gesquière, M. M. Abdel-Mottaleb, S. De Feyter, F. C. De Schryver, M. Sieffert, K. Müllen, A. Calderone, R. Lazzaroni, J.-L. Brédas, *Chem. Eur. J.* **2000**, *6*, 3739–3746.
- [13] S. L. Mayo, B. D. Olafson, W. A. Goddard, III, *J. Phys. Chem.* **1990**, *94*, 8897–8909.

Received: September 21, 2004

Revised: February 18, 2005